Supporting Materials

Dynamic terahertz multi-channel beam steering with dual-frequency multiplexing based on magneto-optical metasurface

Dan Zhao,[a] Fei Fan, [a,b,*] Hao Wang,[a] Pengxuan Li, [a] Zhen Xu, [c] Jining Li, [c, *] Yunyun Ji,[a] Shengjiang Chang [b, *]

[a] Institute of Modern Optics, Nankai University, Tianjin, China, 300350

[b] Tianjin Key Laboratory of Optoelectronic Sensor and Sensing Network Technology, Tianjin, China, 300350

[c] School of Precision Instrument and Optoelectronics Engineering, Institute of Laser and Optoelectronics, Tianjin University, Tianjin 300072, China

*fanfei@nankai.edu.cn

**jiningli@tju.edu.cn

***sjchang@nankai.edu.cn

Section List

1. Detailed sizes of metasurface

The spacing between the rectangular columns in the x and y directions is the same, represented as 450μm. We superimpose the responses of three types of LP states on the metasurface Next, we use the Least Squares Approximation Algorithm to solve the ideal value of the Jones matrix effective unit of each unit in a single period of the metasurface, and then construct the metasurface accordingly. Finally, the specific dimensions of 6×12 meta-atom in the MO metasurface is given in the table as follows.

Table: The specific size of each meta-atom of the MO metasurface

	1			2			3			4			5			6		
	l(μm)	*w*(μm)	*θ*(°)	*l*(μm)	*w*(μm)	*θ*(°)	*l*(μm)	*w*(μm)	*θ*(°)	*l*(μm)	*w*(μm)	*θ*(°)	*l*(μm)	*w*(μm)	*θ*(°)	*l*(μm)	*w*(μm)	*θ*(°)
1	266.2	191.6	-2.0	102.2	101.0	22.5	335.0	105.2	24.2	334.8	105.0	59.6	102.3	100.8	14.2	194.9	268.7	3.6
2	290.8	192.8	37.8	294.2	126.3	38.6	270.2	354.5	24.0	96.5	135.6	43.1	126.4	303.1	-37.9	279.4	344.0	12.8
3	278.9	340.7	76.2	266.5	248.1	57.9	96.7	136.6	47.6	271.6	363.2	71.3	214.8	398.3	19.9	291.0	191.9	49.7
4	317.9	115.1	-48.1	99.4	101.0	18.8	282.2	391.5	-14.7	399.1	280.5	11.7	104.5	102.9	4.6	361.7	176.7	66.7
5	364.3	180.1	22.9	284.9	145.8	32.7	241.0	292.6	68.5	136.0	101.9	27.0	284.4	145.2	58.3	293.1	250.0	-13.5
6	248.6	295.4	13.2	400.5	208.9	37.8	105.6	136.7	-26.2	241.1	291.6	22.6	391.9	211.3	54.2	317.5	118.4	-37.8
7	410.5	85.2	-38.2	83.8	280.0	46.6	273.1	342.2	26.7	342.5	271.0	-33.1	79.2	285.7	49.4	103.3	146.3	11.1
8	367.9	191.8	7.5	83.3	282.0	40.8	275.8	375.6	15.0	104.4	130.2	51.7	81.2	276.1	44.3	283.4	236.9	25.0
9	298.7	240.5	79.6	305.4	240.6	42.7	101.2	126.2	40.0	367.4	277.9	-13.1	306.4	241.1	46.3	214.2	286.2	-23.6
10	329.4	191.6	8.9	104.0	105.0	13.7	102.3	137.1	-28.3	139.7	105.1	28.7	104.0	104.9	2.1	116.9	324.4	50.5
11	372.0	228.3	64.7	276.4	139.7	-34.7	139.8	321.7	63.4	366.8	277.7	23.8	379.8	244.8	43.3	192.6	332.1	-10.6
12	340.4	110.2	-48.1	394.1	218.0	31.0	278.8	360.0	-23.6	312.6	148.4	116.6	203.9	257.5	5.9	295.3	247.5	-8.5

2. Electromagnetic simulation and according results

The numerical simulations in Fig. 2 of the main text are performed by using the finite time domain difference (FDTD) method in the commercial software of Lumerical FDTD Solutions. For the transmittance and phase calculation of the meta-atom, the MPM boundary condition is used for the z direction, and the periodic boundary conditions are applied for the *x*- and *y*-direction. The *y*-LP plane sources vertically incident into the metadevice and the output time-domain signals can be detected with the point detector. The transmittance and the phase for different units can be simulated by Fourier transform according to the electric field at the point monitor. Here, the material Si is set as a loss-free material with the refractive index of 3.4. The diffractive efficiency can be gained from the analysis group from the farfield analysis of the 2-dimensional field monitor. The far-field simulation results are shown in Fig. S1. It's obvious that the output THz wave for the working frequencies of 0.25 THz and 0.5 THz is deflected to (-28°, 0) at B = -0.24 T, (0, 12°) at B = 0 T, (+28°, 0) at B = +0.24 T, which indicates the MO metasurface realizes the dynamical multiplex channel function with dual-frequency multiplexing function.

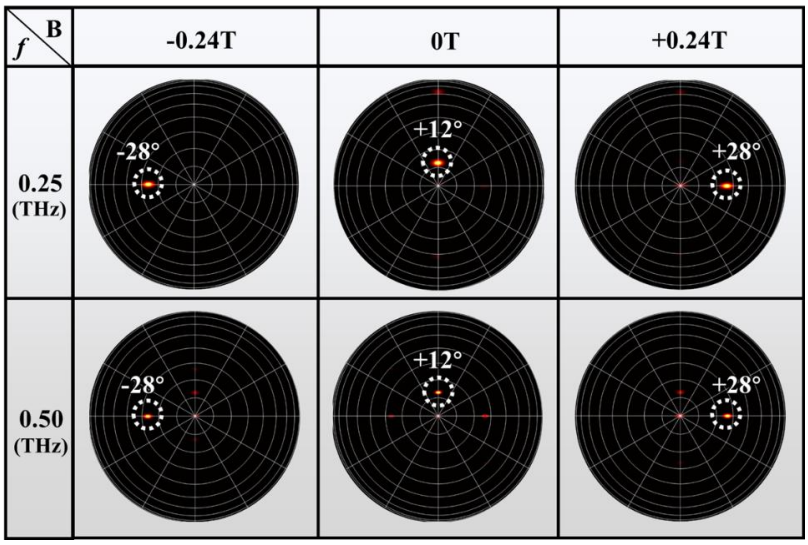

Fig. S1 The simulated results of output farfield at 0.25THz and 0.5THz with different EMFs of +0.24T, 0T, -0.24T.

3. Supplement of experiment results

For the simulation results of Fig. 2 in the main text, we experimentally verified the relationship among the EMFs, frequency, and transmission of the MO metasurface by AR-THz-TDPS. Firstly, the time-domain signal passing through the air and the corresponding frequency-domain spectrum are shown in Fig.S2. The working frequency band of AR-THz-TDPS can cover 0.1 to 1.5 THz.

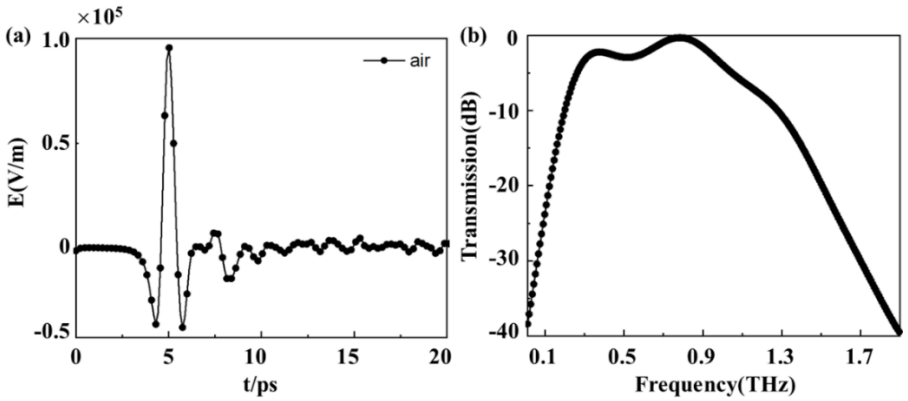

Fig. S2 (a) The time-domain signal of passing through the air; (b) The according frequency spectrum.

Then, the transmission characteristics of the MO metasurface under different EMFs and deflected angles are measured as shown in Fig. S3. As we can see, the experiment results are in good agreement with the simulation results. The deflection angle is (+28°, 0), (+12°, 0), and (-28°, 0) when B = +0.24 T, 0 T, and -0.24 T respectively at dual working frequencies. And, for the deflection angle of (0, -12°), there is no energy is deflected to the angle. Therefore, different deflection channels can be switched by EMFs at dual working frequencies, so the functions of multi-channel multiplexing and dual-frequency multiplexing are proved by experiment results.

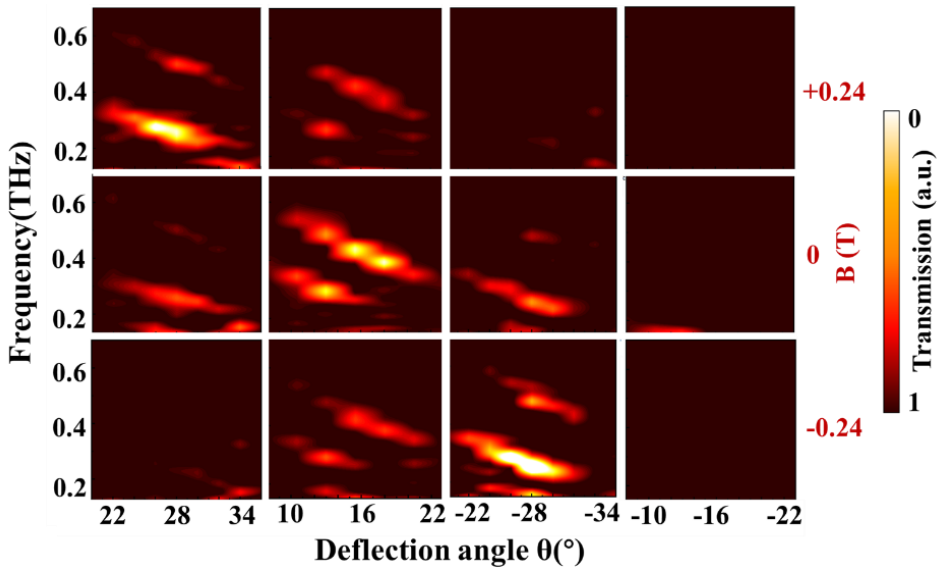

Fig. S3 The experiment transmission results at the frequency band of 0.2 THz ~ 0.65 THz and the deflection angle of (±20°, 0) ~ (±36°, 0), (0, ±8°) ~ (0, ±24°) when B = +0.24 T, 0 T, and -0.24 T.

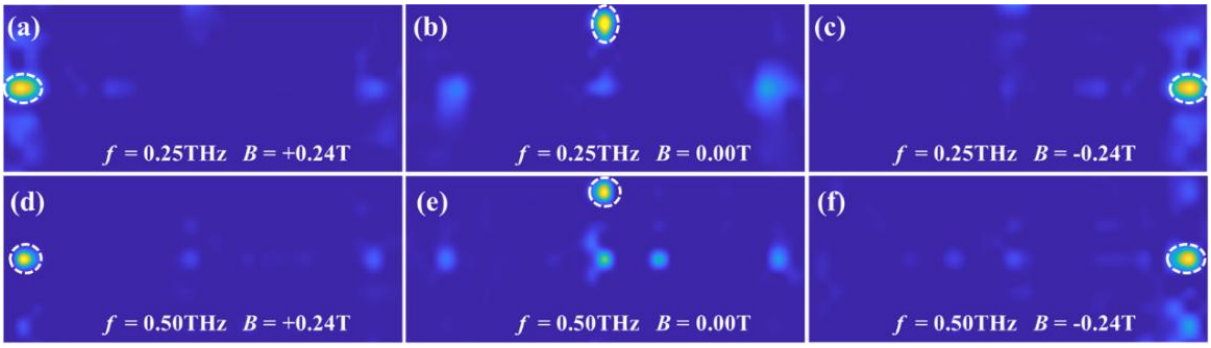

Fig. S4 The experiment far-field distributions at (a) 0.25 THz and +0.24 T, (b) 0.25 THz and 0 T, (c) 0.25 THz and -0.24 T, (d) 0.50 THz and +0.24 T, (e) 0.50 THz and 0 T, (f) 0.50 THz and -0.24 T.

In addition, Fig. S4 shows the distributions of the total far-field electric field when f = 0.25 THz and B = +0.24 T, f = 0.25 THz and B = 0 T, f = 0.25 THz and B = -0.24 T, f = 0.50 THz and B = +0.24 T, f = 0.50 THz and B = 0 T, f = 0.50 THz and B = -0.24 T. It can be seen that the far-field distribution of the total electric field is almost the same as the far-field distribution of the target polarization far-field shown in Fig. 6(a) ~ (f). Then, the proportion of the two situations to describe

the ratio of the target polarization electric field in the total output field. As mentioned in the main text, the ratio of all situations can reach more than 90%. Therefore, the MO metasurface can ensure the low crosstalk between channels and accuracy of the information transmission.

The ratio of the intensity of the target LP state (I_{LP}) to the total intensity of the output electric field at operating EMFs is calculated. And, the ratios of R_{LP} in all situations have been marked on the Fig. S5, with all more than 92%. Therefore, the polarization state of the output THz beam is almost converted into the designed polarization direction as: 0° for Channel 1, 45° for Channel 2, and 90° for Channel 3, respectively, at dual working frequencies.

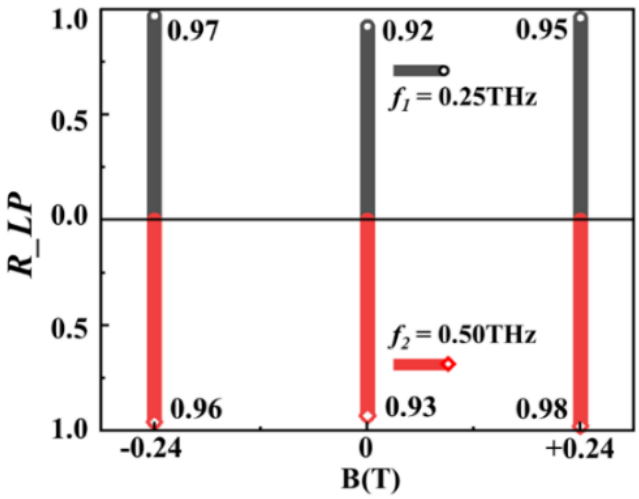

Fig. S5 The ratio of target polarization content to total far-field at 0.25 THz and 0.5 THz at different deflection angles (Φ_1, Φ_2, and Φ_3) and working EMFs.

4. The experiment characteristics of La:YIG crystal

The transmission characteristics of the La:YIG crystal individually is measured when *y*-LP THz wave incidents under different EMFs from -0.26 T to +0.26 T. As shown in Fig. S6(a), when f = 0.25 THz and 0.5 THz, the insertion loss is less than -3 dB, and the absorption coefficient is less than 3 cm^{-1}. In addition, the refractive index is almost constant about 4, and $\Delta n < 0.5$. As shown in Fig. S6(d), the Faraday rotation angle increases gradually with the increase of EMF, and the rotation direction is exactly opposite for the forward and backward EMF. The maximum rotation angle reaches up to 44° at B = +0.26 T in a broadband THz range from 0.2 to 1.1 THz. The above results verify the La:YIG crystal has a low dispersion, a low loss, and high MO coefficient, which make it an ideal candidate functional material for the development of high-performance THz MO devices working at room temperature under a relatively low magnetic field.

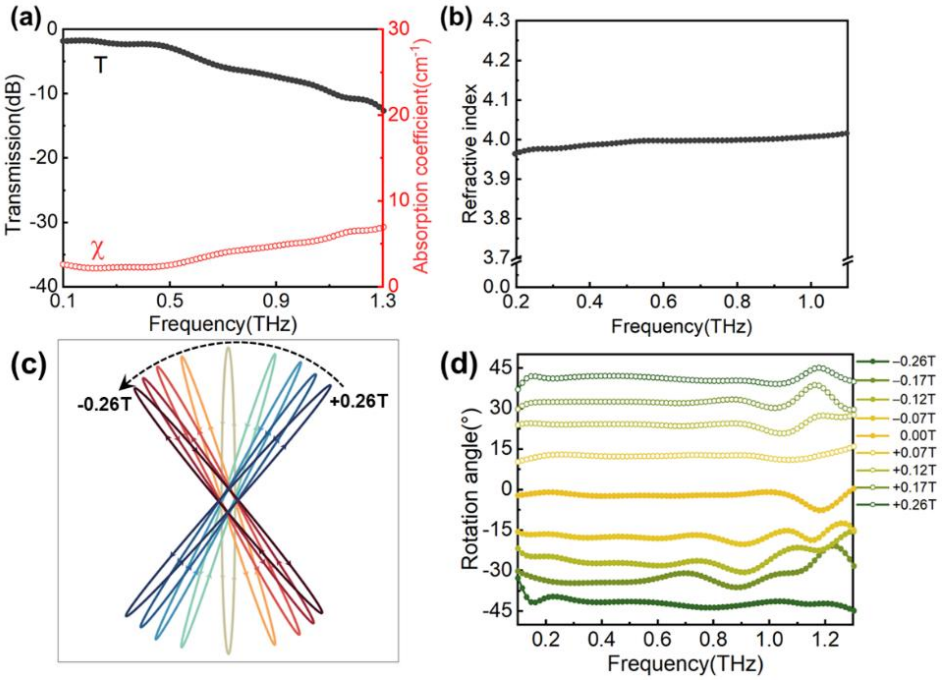

Fig. S6 (a) The transmission and absorption coefficient of the La:YIG crystal; (b) The refractive coefficient of the La:YIG crystal; (c) The output polarization ellipses under different EMFs after y-LP THz wave passing through the La:YIG crystal; (d) The Faraday rotation angles under different EMFs.

5. Introduction of the paraxial approximation

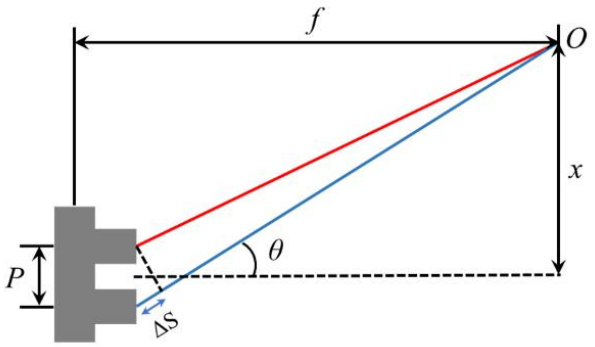

Fig. S7 the transmission paths of two meta-atoms.

We do appreciate the insightful concern about the critical issue. The simple linear superposition of the individual meta-atoms is a paraxial approximation. The actual far field superposition is shown in Fig. S7, which should be strictly expressed as:

$$A_0 \exp(i\varphi_0) = \exp(i\varphi_{i1}) + \exp(i\varphi_{i2}) * \exp\left(i\frac{2\pi}{\lambda}\Delta S\right) \tag{S1}$$

When $\exp(i2\pi\Delta S/\lambda)$ is close to 1, the Eq.(S1) can be simplified through the approximation as follows:

$$A_0 \exp(i\varphi_0) = \exp(i\varphi_{i1}) + \exp(i\varphi_{i2}) \tag{S2}$$

Under this condition, the transmission electric fields of both paths can be roughly calculated by linear superposition. This approximation requires that the optical path difference ΔS be significantly smaller than the wavelength λ ($\Delta S \ll \lambda$). In other words, the approximation condition to consider the output field as the linear superposition of E_{xx1}, E_{yy1}, E_{xy1}, and E_{xx2}, E_{yy2}, E_{yy2} is the paraxial approximation:

$$\Delta S = p\sin\theta \ll \lambda \tag{S3}$$

In this work, the operating frequency is 0.25 THz and 0.5 THz, and the according wavelength is 1200 μm and 600 μm respectively. The period P is 425 μm. And the lens focal length used in the experiment is 25 mm. Obviously, the design and experiment test of the MO device satisfies the approximation condition perfectly. Therefore, the electric field response of each meta-atom can be linearly superimposed, which greatly reduces the amount of calculation and simulation time while ensuring the design accuracy.

6. Error function of the Gradient Descent Algorithm

The error function of the Gradient Descent Algorithm of each meta-atom is defined as

$$\begin{aligned}\sigma &= \sigma_{0.25} + \sigma_{0.5} \\ &= abs\left(E^{0.25}_{xx\_target} - E^{0.25}_{xx}\right) + abs\left(E^{0.25}_{xy\_target} - E^{0.25}_{xy}\right) + abs\left(E^{0.25}_{yy\_target} - E^{0.25}_{yy}\right) \\ &+ abs\left(E^{0.5}_{xx\_target} - E^{0.5}_{xx}\right) + abs\left(E^{0.5}_{xy\_target} - E^{0.5}_{xy}\right) + abs\left(E^{0.5}_{yy\_target} - E^{0.5}_{yy}\right).\end{aligned} \tag{S4}$$

Among that, $E^{0.25/0.5}_{xx\_target}$, $E^{0.25/0.5}_{xy\_target}$, $E^{0.25/0.5}_{yy\_target}$ represents the ideal value of E_{xx}, E_{xy}, E_{yy} calculated by Eqs. (4) ~ (5) of the main text respectively at 0.25 THz and 0.5 THz. In addition, $E^{0.25/0.5}_{xx}$, $E^{0.25/0.5}_{xy}$, $E^{0.25/0.5}_{yy}$ indicates the value of E_{xx}, E_{xy}, E_{yy} at different lengths (l_1, l_2 is set from 50 to 450 μm), widths (w_1, w_2 is set from 50 to 450 μm), and rotation corners (α_1, α_2 is set from –90° to 90°) respectively at 0.25 THz and 0.5 THz. Next, by the Gradient Descent Algorithm and Least Squares Approximation Algorithm, the optimal value of the Jones matrix effective unit which is closest to the ideal value is solved. Then, the sizes of 6×12 meta-atoms are determined. The calculated error of each cell is shown as follows:

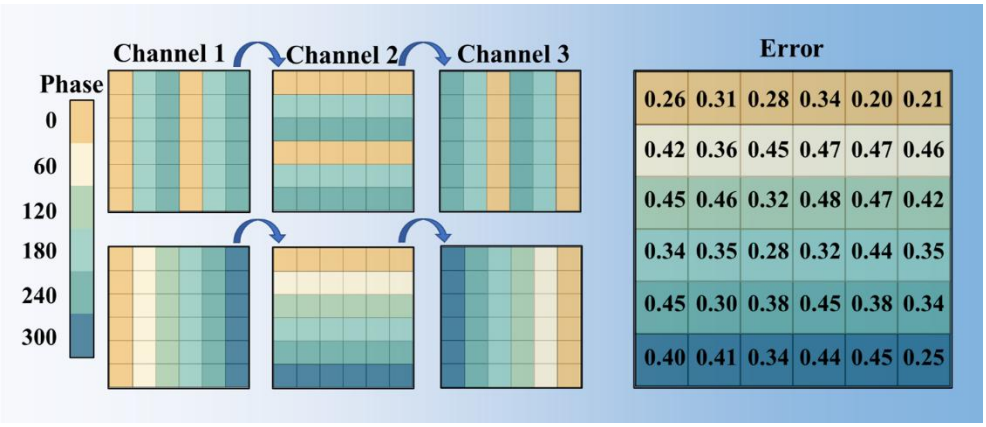

Fig. S8 The calculated error of each cell.

According to Equation (S4), since the value of $|E_{xx}|$, $|E_{xy}|$, and $|E_{yy}|$ all is in the range of -1 to 1, the maximum error is 12. Therefore, the calculated errors all are within 5% of the maximum error, which verifies the rationality of the MO metasurface.